Ceramics International 50 (2024) 14180–14187

Contents lists available at ScienceDirect

Ceramics International

journal homepage: www.elsevier.com/locate/ceramint

Temperature stability, low loss, and phase structure of $MgO–TiO_2$ microwave dielectric ceramic system modified using $Na_{0.5}La_{0.5}TiO_3$

Qi Hu [a,b], Jiayao Liu [a,b], Yuancheng Teng [a,b,*], Fei Zhou [a,b], Xiaofeng Zhao [a,b], Haofeng Jing [a,b], Qingguo Chen [a,b]

[a] State Key Laboratory for Environment-friendly Energy Materials, Southwest University of Science and Technology, Mianyang, 621010, PR China
[b] School of Materials and Chemistry, Southwest University of Science and Technology, Mianyang, 621010, PR China

ARTICLE INFO

Handling Editor: Dr P. Vincenzini

Keywords:
$MgO-TiO_2$
$Na_{0.5}La_{0.5}TiO_3$
Temperature stability
Phase structure

ABSTRACT

$MgTiO_3–Mg_2TiO_4–Na_{0.5}La_{0.5}TiO_3$ (MMNL) microwave ceramics were prepared using a conventional solid-state method. The stability of dielectric properties was investigated over a wide range of temperatures. The effects of the composition of the three phases on the microwave dielectric properties of the MMNL ceramics were investigated. The results showed that a high sintering temperature reduces the structural stability and compactness of the ceramics, leading to a deterioration in their dielectric properties. The addition of $MgTiO_3$ effectively increased the vibration peak intensity of the $[TiO_6]$ oxygen octahedra but reduced the relative density, leading to a decrease in the $Q \times f$ value. The τ_f value approached zero in a wide temperature range (−40–120 °C) by regulating the phase compositions of the MMNL ceramics. In particular, the $0.21MgTiO_3$-$0.653Mg_2TiO_4$-$0.137Na_{0.5}La_{0.5}TiO_3$ ceramic sintered at 1440 °C for 6 h exhibited superior microwave dielectric properties: $\varepsilon_r = 17.5$ (8.83 GHz), $Q \times f = 62{,}800$ GHz, and $\tau_f = -0.35$ ppm/°C.

1. Introduction

Microwave dielectric ceramics (MWDCs) play an important role in 5G devices. With the development of 5G techniques, the pursuit of high-performance MWDCs with low dielectric loss, a suitable dielectric constant, and the temperature coefficient of the resonant frequency approaching zero is a major objective for obtaining high-performance 5G devices [1]. To satisfy the working temperature change in global area, MWDC devices should have good temperature stability in the range of −40 °C to 120 °C [2,3]. Currently, for regulating the temperature coefficient of the resonant frequency, the positive temperature range of the τ_f value is primarily considered, while the negative temperature range is always neglected [4]. Ceramics with the temperature coefficient of the resonant frequency approaching zero over wide temperature ranges (−40–105 °C and −55–85 °C) were prepared via stacking sintering and non-stoichiometric unequal incorporation of elements; however, these methods involve complex processes and high costs. In addition, the material must have a high thermal expansion coefficient [2–5].

Because of their low dielectric constant, high quality factor, low costs, and abundantly available raw materials, $MgO–TiO_2$-based (such as $MgTiO_3$ and Mg_2TiO_4) microwave dielectric ceramics have attracted extensive attention in the 5G communication industry; however, their large τ_f value limits their practical application [5–7]. Two-phase mixtures with positive τ_f materials, such as $CaTiO_3$, $SrTiO_3$, $Ca_{0.8}Sr_{0.2}TiO_3$, $NaTaO_3$, and $MgTa_2O_6$, as temperature compensators were proposed to adjust the τ_f value to zero in the temperature range of 25~85 °C [8–16]. Furthermore, researchers have tried to improve the dielectric properties of $MgO–TiO_2$ ceramics by incorporating a third phase; however, these ceramics did not show good temperature stability in the range of −40–120 °C [17–20]. $Na_{0.5}La_{0.5}TiO_3$ ($\varepsilon_r = 122$, $Q \times f = 9800$ GHz, and $\tau_f = +480$ ppm/°C) exhibits a low dielectric loss [21] and is a potential candidate to compensate for the negative τ_f value of the $MgO–TiO_2$ ceramics. Previous studies have shown that the τ_f values of the $Na_{0.5}La_{0.5}TiO_3–MgTiO_3$ and $Na_{0.5}La_{0.5}TiO_3–Mg_2TiO_4$ ceramics prepared via simple mixing tended toward zero at high temperatures; however, they showed a high negative value at a low temperature [4,20,22]. Hence, in this study we propose to use multiphase mixing to obtain the near zero τ_f value in wider temperature ranges, which is of immense significance for investigating the dielectric properties of the three

* Corresponding author.State Key Laboratory for Environment-friendly Energy Materials, Southwest University of Science and Technology, Mianyang, 621010, PR China.
E-mail address: Teng_TG314@163.com (Y. Teng).

https://doi.org/10.1016/j.ceramint.2024.01.324
Received 12 June 2023; Received in revised form 23 January 2024; Accepted 23 January 2024
Available online 24 January 2024

elementary multiphase ceramics by adjusting the ratio of the components.

Therefore, we prepared $MgTiO_3$–Mg_2TiO_4–$Na_{0.5}La_{0.5}TiO_3$ (MMNL) ceramics using a conventional solid-phase mixing method. The effects of the composition of the three phases on the dielectric properties of MMNL ceramics were studied. The MWDCs with good dielectric temperature stability over a wide range (−40–120 °C) will be further investigated.

2. Experimental procedure

Analytically pure Na_2CO_3 (99 %), La_2O_3 (99.9 %), TiO_2 (99 %), and MgO (98 %) from Sinopharm Chemical Reagent Corporation (Shanghai, China) were selected as initial raw materials and weighed according to the chemical formulas of $Na_{0.5}La_{0.5}TiO_3$, Mg_2TiO_4, and $MgTiO_3$. The raw material mixture was ball milled in a milling jar for 3 h using anhydrous ethanol as the dispersant. The material:ethanol:ball ratio was 1:1.2:3, the speed was 350 rpm, and the grinding ball used was zirconium oxide. The resultant slurry was baked at 60 °C for 12 h and then crushed. The $Na_{0.5}La_{0.5}TiO_3$, Mg_2TiO_4, and $MgTiO_3$ raw materials were individually placed in a ceramic fiber furnace and calcined at 1100, 1250, and 1150 °C for 1 h, respectively. After each calcined powder was ground into particles using an agate mortar, it was weighed and mixed in a ball mill jar in the desired ratio and ball milled for 3 h using deionized water as the dispersant. The resultant slurry was placed in an evaporating dish and baked at 60 °C for 12 h. Subsequently, a powder mass fraction of 1 wt% of adhesive (PVA solution) was added to it. The granulated powder was then passed through a 50–100 mesh sieve. The resultant powder was pressed into small cylindrical pieces of 6.4–6.6 mm thickness at 250 MPa using a 13 mm steel die mold. The sample discs were placed in alumina porcelain boats and sintered in a ceramic fiber furnace. The sintering regime included a heating rate of 5 °C/min, holding at 600 °C for 2 h for degumming, and then increasing to a different temperature for sintering for 6 h to obtain the ceramic samples, which were then polished using a metallographic polishing machine and placed in an ultrasonic cleaner for 20 min. After baking at 90 °C for 24 h, the samples were thermally etched for 30 min at 150 °C below the sintering temperature.

The crystalline phases of the sintered samples were analyzed using X-ray diffraction (XRD, XPert Pro, PANalytical, Netherlands). Their microstructures were studied using high-resolution cold-field-emission scanning electron microscopy (CFE-SEM, UItra55, Zeiss, Germany) along with energy-dispersive spectrometry (EDS). A laser Raman spectrometer (InVia, Renishaw, UK) was used for spectral vibration mode analysis. The valence states and bonding structures of the elements were analyzed using X-ray photoelectron spectroscopy (XPS, ESCALAB 250Xi, Thermo Fisher Scientific, USA). The microwave dielectric properties were measured in the TE_{011} mode using a network analyzer (E5071C, Agilent Technologies, USA) according to the Hakki−Coleman method. The test system consisted of a dielectric resonator and a wide temperature cabinet. The resonant frequency corresponding to each temperature was obtained under the conditions of −40 and 120 °C for 30 min to determine the temperature coefficient of the resonant frequency (τ_f) using Eq. (1).

$$\tau_f = \frac{f_{120}\text{-}f_{\text{-}40}}{f_{\text{-}40}(T_{120}\text{-}T_{\text{-}40})} \times 10^6 \ (\text{ppm}\backslash/^\circ\text{C}) \quad (1)$$

where f_{120} and $f_{\text{-}40}$ correspond to the resonant frequencies of the sample in the TE_{011} mode at 120 and −40 °C, respectively. The apparent density was measured using the Archimedes' drainage method; the relative density (ρ_{re}) is the ratio of the measured density (ρ_{bu}) to the theoretical density (ρ_{th}), which in turn was determined using Eq. (2).

$$\rho_{th} = V_{M1} \times \rho_{M1} + V_{M2} \times \rho_{M2} + V_{NL} \times \rho_{NL} \quad (2)$$

where V_{M1}, V_{M2}, and V_{NL}, and are the volume fractions and ρ_{M1}, ρ_{M2}, and ρ_{NL} are the theoretical densities of $MgTiO_3$, Mg_2TiO_4, and $Na_{0.5}La_{0.5}TiO_3$, respectively. The measured density (ρ_{re}) was calculated using Eq. (3).

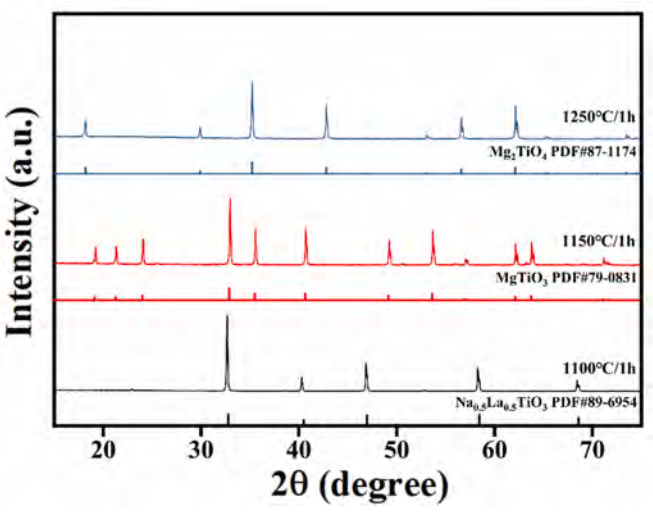

Fig. 1. XRD patterns of the calcined powder of each component.

$$\rho_{bu} = \frac{m_d}{m_d\text{-}m_w} \times \rho_w \quad (3)$$

where m_d, m_w, and ρ_w are the mass of the sample in the dry state, the mass of the sample immersed in water, and the water density at the time of measurement, respectively.

3. Results and discussion

The XRD patterns of the $Na_{0.5}La_{0.5}TiO_3$, $MgTiO_3$, and Mg_2TiO_4 powders are shown in Fig. 1. The diffraction peaks of the three components were consistent with the PDF cards of $Na_{0.5}La_{0.5}TiO_3$, $MgTiO_3$, and Mg_2TiO_4, and no other miscellaneous phases were observed. These results show that $Na_{0.5}La_{0.5}TiO_3$, $MgTiO_3$, and Mg_2TiO_4 were successfully synthesized via calcination at 1100, 1150, and 1250 °C, respectively.

According to the dielectric property parameters of each single-phase ceramic obtained from the experiment, the temperature coefficient of the resonant frequency approached zero when the composition of the MMNL composite ceramic was $0.23MgTiO_3$-$0.633Mg_2TiO_4$-$0.137Na_{0.5}La_{0.5}TiO_3$ (M23MNL137). Fig. 2 shows the XRD patterns of the M23MNL137 ceramics sintered at different temperatures (1320–1500 °C). The diffraction patterns of all samples sintered at different temperatures showed pure crystal phases of $Na_{0.5}La_{0.5}TiO_3$, $MgTiO_3$, and Mg_2TiO_4, and are in accordance with those of $Na_{0.5}La_{0.5}TiO_3$ (PDF#89–6954), $MgTiO_3$ (PDF#79–0831), and Mg_2TiO_4 (PDF#87–1174). However, the diffraction peak intensities decreased with increasing sintering temperature, indicating the formation of a glass phase. $MgTiO_3$, $Na_{0.5}La_{0.5}TiO_3$, and Mg_2TiO_4 do not form solid solutions because of their different crystal structures: $MgTiO_3$, $Na_{0.5}La_{0.5}TiO_3$, and Mg_2TiO_4 have ilmenite-, perovskite-, and spinel-type crystal structures, respectively [23].

The densities of the M23MNL137 ceramics sintered at different temperatures are shown in Fig. 3 and, the SEM images (inset) show the surface morphology of the samples sintered at 1320, 1380, 1440, and 1500 °C. With an increase in the sintering temperature, the density of the M23MNL137 ceramics first increased, then gradually decreased, and finally attained the maximum value at 1440 °C. Notably, the grain size of the M23MNL137 ceramics was relatively small with more pores and a low density when the sintering temperature was 1320 °C. The densification of the ceramics was significantly improved owing to an increase in the sintering force with an increase in the sintering temperature,

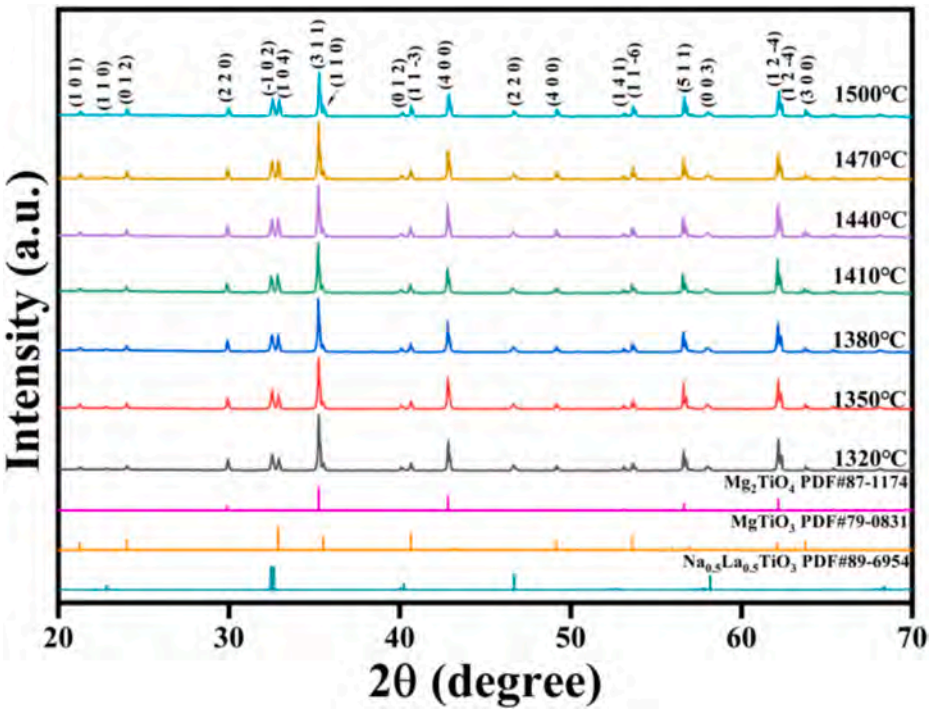

Fig. 2. XRD patterns of the M23MNL137 ceramics sintered at different temperatures.

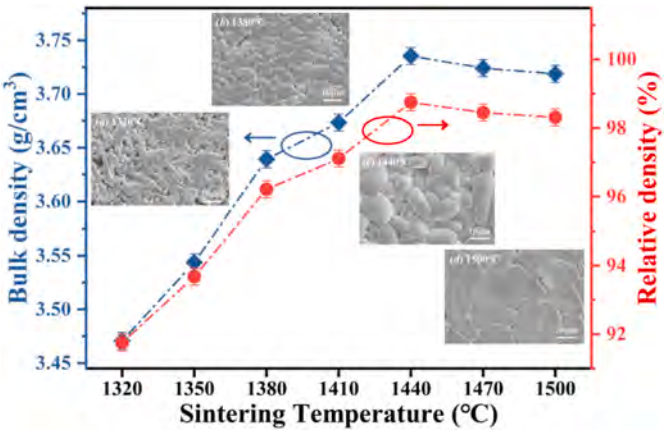

Fig. 3. Surface morphology and density curves of the M23MNL137 ceramics sintered at different temperatures.

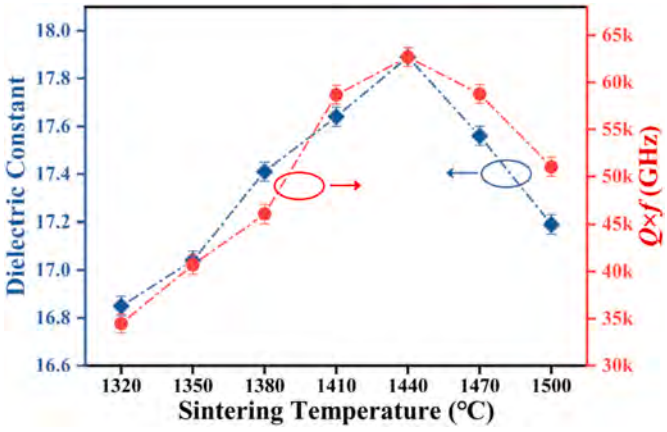

Fig. 4. Dielectric properties of the M23MNL137 ceramics sintered at different temperatures.

resulting in a larger grain size and reduced pores between the grains [24]. Ceramic samples sintered at 1440 °C exhibited the highest density, a relative density of 98.75 %, and an average grain size of approximately 12 μm. Further increasing the sintering temperature leads to an abnormal grain growth of more than 20 μm and an increased amount of glass phase, which is attributed to over-sintering [25].

Fig. 4 shows the dielectric properties of the M23MNL137 ceramics sintered at different temperatures. The variation in their dielectric properties with the sintering temperature is consistent with the evolutionary trend observed for their density, as shown in Fig. 3. The compactness of ceramics is a crucial factor that affects their dielectric properties [26,27]. Ceramic samples sintered at low temperatures are less dense and more porous, thus exhibiting a low dielectric constant and high dielectric loss. Over-sintering leads to an abnormal grain growth and increased the amount of the glass phase in the samples. An active crystal structure with a poor lattice stability results in the deterioration of dielectric properties.

It has been reported that the valence state of Ti in ceramics transforms from Ti^{4+} to Ti^{3+} under a high-temperature reduction reaction, which affects their dielectric properties [28,29]. Therefore, XPS analysis was performed to investigate the effects of sintering temperature on the crystal binding energy and the valence state of Ti. Fig. 5 shows the XPS profiles of Ti and O in the M23MNL137 ceramics sintered at different temperatures. As shown in Fig. 5(a), two peaks corresponding to O(I) and O(II) were obtained by fitting the XPS peaks. The O(I) peak at 529.3 eV corresponds to lattice oxygen, while the O(II) peak at 530.9 eV is due to several oxygen-containing groups such as O_2, H_2O, OH and other physical and chemical adsorption [30,31]. The results showed that the peak ratio of O(I) to O(II) attained the maximum value when the sintering temperature was 1440 °C, indicating a stronger metal-O bonding in the ceramics. The peaks at binding energies of 464.5 and 458.9 eV correspond to Ti^{4+} $2p_{1/2}$ and Ti^{4+} $2p_{3/2}$, respectively [20,32]. The binding energy of the peaks corresponding to Ti^{3+} $2p_{3/2}$ and Ti^{3+} $2p_{1/2}$ was 457.4 and 463.1 eV, respectively [33]. As shown in Fig. 5(b), increasing the sintering temperature did not convert Ti^{4+} into Ti^{3+} in the

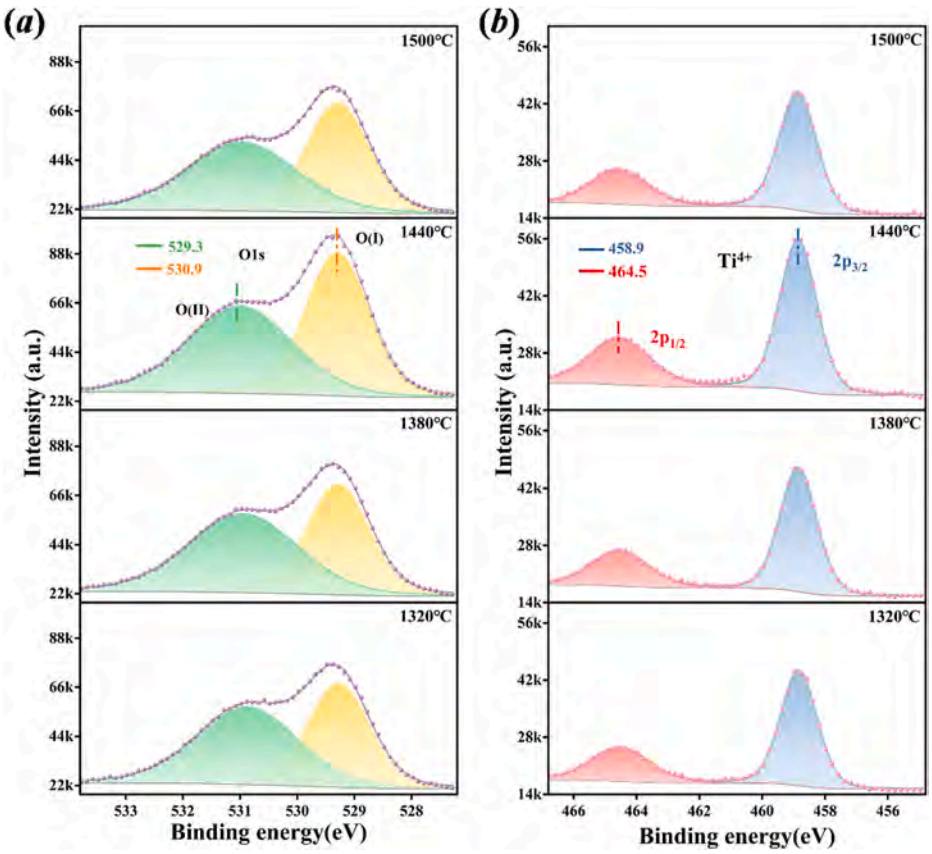

Fig. 5. XPS profiles of Ti and O in the M23MNL137 ceramics sintered at different temperatures.

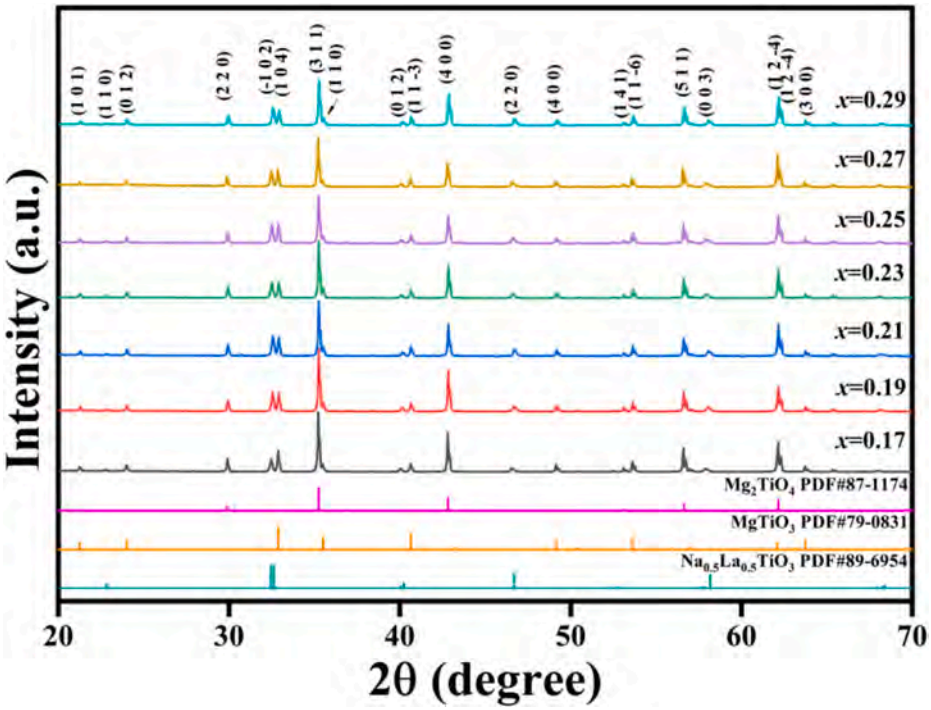

Fig. 6. XRD patterns of the M*x*MNL137 (x = 0.17, 0.19, 0.21, 0.23, 0.25, 0.27, 0.29) ceramics sintered at 1440 °C.

M23MNL137 ceramics. However, a high temperature reduces the crystal stability, which is one of the factors leading to a decrease in the dielectric properties.

Based on the analysis results of the crystal structure, microstructure, relative density, grain size, and dielectric properties of the M23MNL137 ceramics sintered at different temperatures, it was found that the ideal

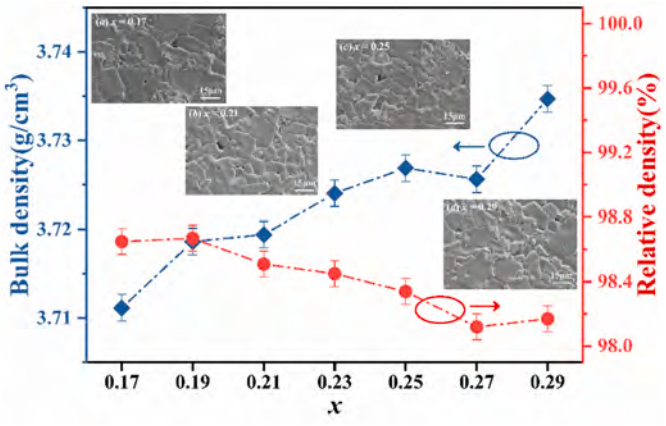

Fig. 7. Surface morphology and density curves of the M*x*MNL137 (x = 0.17, 0.21, 0.25, 0.29) ceramics sintered at 1440 °C.

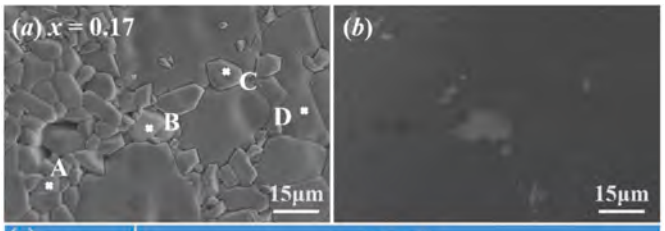

(c)

Elements	Atom %			
	A	B	C	D
Na	0	8.75	0	0
La	0	9.12	0	0
Ti	17.16	16.21	16.73	12.16
Mg	17.89	0	18.48	23.89
O	64.95	65.92	64.79	63.95

Fig. 8. Surface morphology and EDS analysis of the M17MNL137 ceramics: (a) SEM and (b) BSE images; (c) EDS results.

sintering temperature for the MMNL ceramics was 1440 °C.

In addition to the sintering temperature, the phase component is another key factor that affects the dielectric properties of ceramics. Fig. 6 shows the XRD patterns of the xMgTiO$_3$-(0.6333−x)Mg$_2$TiO$_4$-0.137Na$_{0.5}$La$_{0.5}$TiO$_3$ (M*x*MLN137) (x = 0.17, 0.19, 0.21, 0.23, 0.25, 0.27, 0.29) ceramics. Notably, the phase structures of MgTiO$_3$, Mg$_2$TiO$_4$, and Na$_{0.5}$La$_{0.5}$TiO$_3$ did not change with variation in the MgTiO$_3$ content, indicating that the change in the component content has no noticeable effect on the phase structure of the MMNL ceramics. With an increase in the MgTiO$_3$ content (x), the strongest diffraction peak intensity corresponding to MgTiO$_3$ increased, while that corresponding to Mg$_2$TiO$_4$ decreased, and that of Na$_{0.5}$La$_{0.5}$TiO$_3$ remained basically unchanged, which is consistent with the actual phase composition results of the MMNL ceramics.

Fig. 7 shows the surface topography and density variation of the M*x*MNL137 (x = 0.17, 0.21, 0.25, 0.29) ceramics sintered at 1440 °C. They exhibited good crystallinity at 1440 °C. When the content of MgTiO$_3$ was 0.17, the grain uniformity was poor owing to the high content of Mg$_2$TiO$_4$ inhibiting the growth of the other phases. When x = 0.21, the grain uniformity was considerably improved, indicating that an appropriate amount of MgTiO$_3$ can inhibit the growth of Mg$_2$TiO$_4$ grains in the MMNL ceramics; however, the porosity increased. Na$_{0.5}$La$_{0.5}$TiO$_3$ was the only minor phase when x was between 0.21 and 0.29, and the crystal uniformity of MMNL decreased, accompanied by the formation of large grains. Moreover, the density evolution analysis

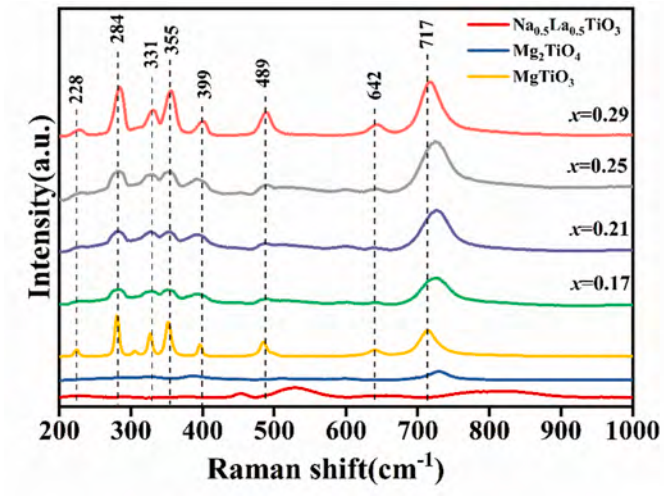

Fig. 9. Raman spectra of the M*x*MNL137 (x = 0.17, 0.21, 0.25, 0.29) ceramics sintered at 1440 °C.

showed that the bulk density increased; however, the relative density decreased, which is consistent with the microscopic morphological analysis results.

To obtain the microstructural distributions of MgTiO$_3$, Mg$_2$TiO$_4$, and Na$_{0.5}$La$_{0.5}$TiO$_3$ in the ceramic samples, backscattered electron (BSE) images and EDS results were obtained for the ceramic samples, which are shown in Fig. 8. Fig. 8(a) and (b) show smaller and fewer Na$_{0.5}$La$_{0.5}$TiO$_3$ particles for a lower content of Na$_{0.5}$La$_{0.5}$TiO$_3$. Fig. 8(c) shows the EDS analysis results of the grains of different sizes [as indicated in Fig. 8(a)]. In Fig. 8(a), points A and B correspond to the MgTiO$_3$ grains, indicating that the grains of MgTiO$_3$ are small for a low additive content. Point C is indexed to a Na$_{0.5}$La$_{0.5}$TiO$_3$ grain, in which only a small degree of volatilization of Na can be observed. Point D is indexed to a Mg$_2$TiO$_4$ grain, which appears relatively large because of its high additive content. It was further verified that the grain boundaries of the Mg$_2$TiO$_4$ grains in the ceramic samples prevented the grain boundary motion of other grains and hindered the grain growth, leading to differences in the grain size [34].

Fig. 9 shows the Raman spectra of the M*x*MNL137 (x = 0.17, 0.21, 0.25, 0.29) ceramics in the range of 200–1000 cm^{-1}. Because of the overlapping of vibration modes with similar frequencies from the three different components, only eight major Raman peaks were observed. The Raman vibration mode of the MMNL ceramics was mainly ascribed to MgTiO$_3$, and no new vibration mode was observed, indicating that no other phase was generated. At low MgTiO$_3$ contents, Na$_{0.5}$La$_{0.5}$TiO$_3$ exhibited a weak peak, which was gradually covered with increasing MgTiO$_3$ content. The highly covalent Ti–O bond dominated the Raman vibration and [TiO$_6$] octahedral symmetric tensile vibration appeared at 717 cm^{-1} [35,36].

Fig. 10(a) shows the variation curves of the dielectric constants of the M*x*MNL137 (x = 0.17, 0.19, 0.21, 0.23, 0.25, 0.27, 0.29) ceramics sintered at different temperatures. The results suggest that the density and phase composition are the two main factors affecting the dielectric properties. The lower porosity and higher density of the samples resulted in a better dielectric constant and quality factor. The evolutionary tendency of the dielectric constant of all the M*x*MNL137 (x = 0.17, 0.19, 0.21, 0.23, 0.25, 0.27, 0.29) samples is consistent with the density variation trend shown in Fig. 3. The maximum value of dielectric constant was obtained at 1440 °C, indicating the best sintering densification. At a constant sintering temperature, the phase composition is the most important factor affecting the dielectric properties. As the dielectric constant ε_r of single-phase Mg$_2$TiO$_4$ ceramics is smaller than that of MgTiO$_3$, the Lichtenecker rule predicts that the dielectric constant of the MMNL ceramics will increase with an increase in the phase fraction of

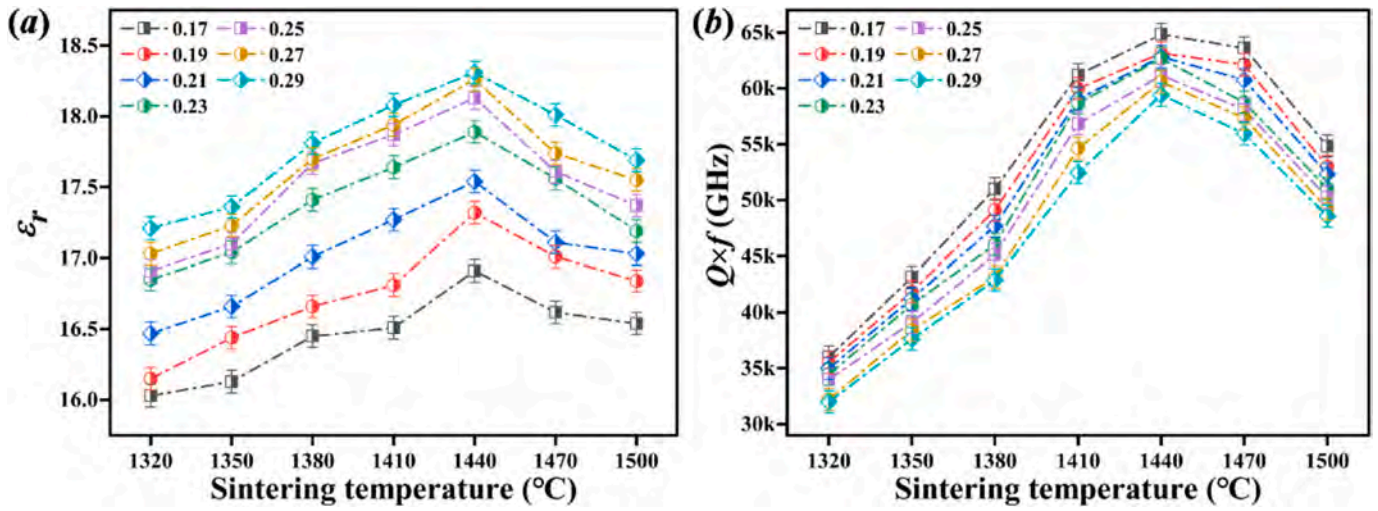

Fig. 10. Dielectric properties of the M*x*MNL137 (x = 0.17, 0.19, 0.21, 0.23, 0.25, 0.27, 0.29) ceramics sintered at different temperatures.

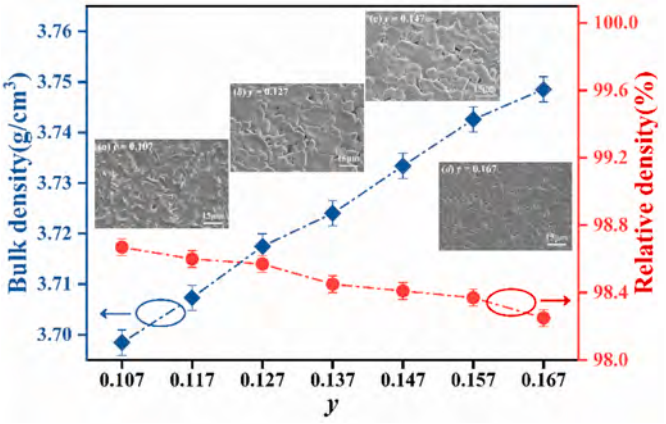

Fig. 11. Surface morphology and density curves of M23M633NLy (y = 0.107, 0.117, 0.127, 0.137, 0.147, 0.157, 0.167) ceramics sintered at 1440 °C.

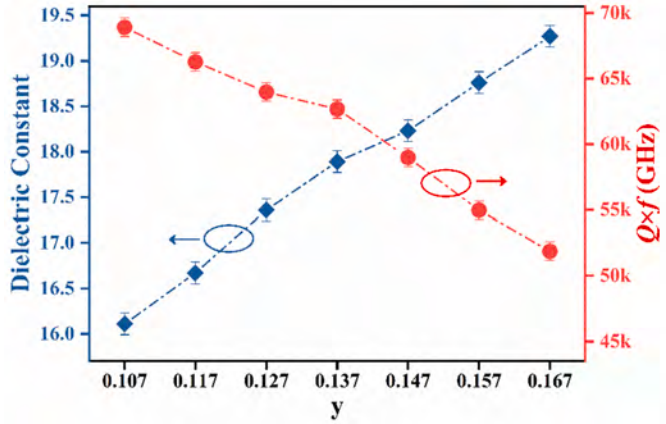

Fig. 12. Dielectric properties of the M23M633NLy (y = 0.107, 0.117, 0.127, 0.137, 0.147, 0.157, 0.167) ceramics sintered at 1440 °C.

$MgTiO_3$ [37,38]. Fig. 10(b) shows the quality factor Q × f value of the MMNL ceramics with different contents of $MgTiO_3$, which is consistent with the density variation trend shown in Fig. 3. This indicates that the effects of the sintering temperature on the density of the ceramics within a certain range do not change. The Q × f value of microwave dielectric ceramics is not only affected by the oxygen octahedral vibration but is also related to the relative density. A lower density leads to a smaller reduction in the dielectric properties and dielectric loss [39,40]. Fig. 9 shows that the [TiO_6] octahedral symmetric tensile vibration peak of the M*x*MNL137 ceramics becomes narrow with increasing x. In contrast, the relative density of the M*x*MNL137 ceramics decreased with increasing x (Fig. 7). Moreover, when x was between 0.17 and 0.29, the Q × f value of the MMNL ceramics decreased with increasing $MgTiO_3$ content.

Fig. 11 shows the surface morphology and density change curves of the 0.23$MgTiO_3$-0.633Mg_2TiO_4-$y$$Na_{0.5}La_{0.5}TiO_3$ (M23M633NLy) (y = 0.107, 0.117, 0.127, 0.137, 0.147, 0.157, 0.167) ceramics sintered at 1440 °C. The microscopic surface morphology and relative density of the M23M633NLy ceramics appreciably changed with variation in the $Na_{0.5}La_{0.5}TiO_3$ content; however, the relative densities of all ceramic samples were more than 98 %. When y = 0.107, the Mg^{2+} and $(Na_{0.5}La_{0.5})^{2+}$ ions exhibited a large difference and could not form a solid solution, indicating that the $Na_{0.5}La_{0.5}TiO_3$ grains are in the large grain gap of Mg_2TiO_4 [41]. The ceramic sample had a relatively small grain size, few pores, compact grain size, and high relative density. With increasing $Na_{0.5}La_{0.5}TiO_3$ content, the degree of grain refinement and uniformity between the grains increased. Although the volume density increased, the porosity also increased. Hence, the relative density and compactness decreased. When y was 0.167, the ceramic grains became very small, indicating that the grain size of M23M633NLy first increased and then decreased with an increase in the content of $Na_{0.5}La_{0.5}TiO_3$ within the experimental range. For ceramic samples with a three-phase coexistence, the grain growth is affected by many factors. The change in components binds grain boundaries and hinders their diffusion, leading to the refinement of ceramic grains.

The dielectric properties of the M23M633NLy ceramics sintered at 1440 °C are shown in Fig. 12. When the content of $Na_{0.5}La_{0.5}TiO_3$ ranged from 0.107 to 0.167, the dielectric constant and quality factor changed significantly. The dielectric constant value increased from 16.1 to 19.3 because the polarizability of $Na_{0.5}La_{0.5}TiO_3$ was larger than those of $MgTiO_3$ and Mg_2TiO_4. However, $Na_{0.5}La_{0.5}TiO_3$ has a high dielectric constant and its dielectric loss is relatively large, which decreases the quality factor of the MMNL ceramics [20]. With an increase in the content of $Na_{0.5}La_{0.5}TiO_3$ (y), the Q × f value decreased from 68, 900 GHz to 51,900 GHz. Therefore, it is necessary to reasonably regulate the components and synthesis parameters to achieve excellent dielectric properties.

Fig. 13(a) and (b) show the τ_f values of the M*x*MNL137 ceramics and M23M633NLy ceramics with varying x and y in the temperature range of −40 °C to 120 °C, respectively. The temperature coefficients of $MgTiO_3$ and Mg_2TiO_4 are complementary at both high and low temperatures. As

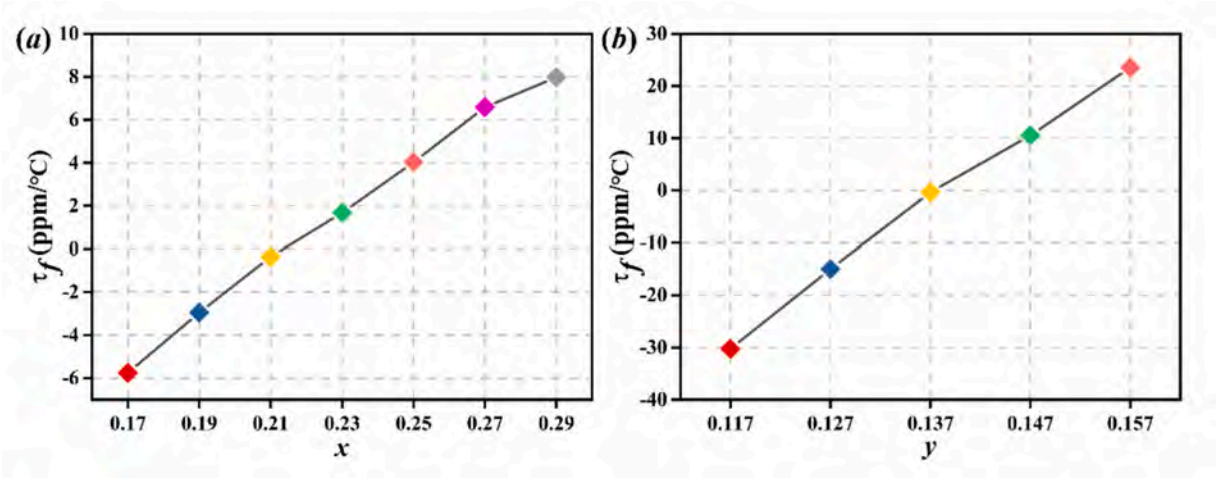

Fig. 13. τ_f values of the MMNL ceramics with different component contents in the temperature range of −40 °C to 120 °C.

Table 1
Comparison of the microwave dielectric properties of several MgO–TiO_2-based MWDC materials.

Materials	ε_r	Q × f	τ_f (ppm/°C)	Temperature range	Reference
0.93 [0.95Mg_2TiO_4–0.05Co_2TiO_4]-0.07$CaTiO_3$	17	90,000	−5	20~80 °C	[42]
0.8$MgTiO_3$-0.2$Mg_{2.05}SiO_{4.05}$-0.06$CaTiO_3$	15.4	72,705	−1.5	20~80 °C	[43]
$Mg_6Ti_5O_{16}$	16.7	143,481	−51.5	25~85 °C	[44]
$Mg_6Ti_5O_{16}$ doped with 0.35 Ca^{2+}	19.87	100,432	−3	25~85 °C	[17]
1 wt%ZnO–$Mg_{1.15}Ca_{0.05}TiO_{3.6}$	20.3	64,740	−1.3	25~85 °C	[19]
0.78$Mg_6Ti_5O_{16}$-0.22$Ca_{0.8}Sr_{0.2}TiO_3$	20.25	74,200	−1.28	25~85 °C	[18]
0.2$MgTiO_3$-0.56Li_2TiO_3-0.2$MgTiO_3$	21.2	80,000	2.7/-3	−40–105 °C	[4]
0.32Mg_2TiO_4-0.611$MgTiO_3$-0.069$CaTiO_3$	19.7	55,400	4.5/−5.1	−40–90 °C	[20]
0.21$MgTiO_3$-0.653Mg_2TiO_4-0.137$Na_{0.5}La_{0.5}TiO_3$	17.5	62,800	−0.35	−40–120 °C	This study

an excellent compensator for the temperature coefficient of resonant frequency with a large positive τ_f value, increasing the content of $Na_{0.5}La_{0.5}TiO_3$ in the MMNL ceramics changes the τ_f value to positive. Previous studies have shown that the addition of $Na_{0.5}La_{0.5}TiO_3$ can regulate the value of τ_f in MgO–TiO_2 ceramics (Table 1). When $x = 0.21$ and $y = 0.137$, the MMNL ceramics exhibited the highest τ_f value tending to zero ($\tau_f = -0.35$ ppm/°C) in the temperature range from −40 °C to 120 °C.

4. Conclusion

In this study, the dielectric properties of the MxMNL137 (x = 0.17, 0.19, 0.21, 0.23, 0.25, 0.27, 0.29) ceramics sintered at different temperatures (1320, 1350, 1380, 1410, 1440, 1470, and 1500 °C) and M23M633NLy (y = 0.107, 0.117, 0.127, 0.137, 0.147, 0.157, 0.167) ceramics sintered at 1440 °C were investigated. The XRD patterns showed that the three phases coexisted and no other heterophases were produced. High temperatures led to the formation of a glass phase, which reduced the lattice stability and density, resulting in the deterioration of the dielectric properties. The SEM images showed that the addition of low amounts of $MgTiO_3$ and $Na_{0.5}La_{0.5}TiO_3$ played an important role in the physical properties of the MMNL multiphase ceramics. The smaller the difference in composition, the more distinct the grain refinement. Mg_2TiO_4, $MgTiO_3$, and $Na_{0.5}La_{0.5}TiO_3$ exhibited the same synergistic effect in improving the microwave dielectric properties of the MMNL ceramics. Mg_2TiO_4 effectively increased the Q × f value of the MMNL ceramics, but slightly decreased the ε_r value. $MgTiO_3$ increased the vibration peak intensity of the [TiO_6] oxygen octahedron but reduced the relative density, resulting in a decrease in the Q × f value. $Na_{0.5}La_{0.5}TiO_3$ drastically increased the ε_r value of the MMNL ceramics; however, the Q × f value drastically decreased. In conclusion, the results show that the three-phase regulation achieved the objective of fabricating MMNL ceramics with τ_f values tending towards zero in the wide temperature range of −40–120 °C. The 0.21$MgTiO_3$-0.653Mg_2TiO_4-0.137$Na_{0.5}La_{0.5}TiO_3$ ceramic sintered at 1440 °C for 6 h exhibited superior microwave dielectric properties: ε_r = 17.5 (8.83 GHz) , Q × f = 62,800 GHz, and τ_f = −0.35 ppm/°C.

Data availability

The authors declare that the data supporting the findings of this study are available within the article. No new data were created during the study.

Declaration of competing interest

We declare that we have no financial and personal relationships with other people or organizations that can inappropriately influence our work, there is no professional or other personal interest of any nature or kind in any product, service and/or company that could be construed as influencing the position presented in, or the review of, the manuscript entitled,"**Temperature stability, low loss and phase structure of MgO–TiO_2 microwave dielectric ceramic system modified** using **$Na_{0.5}La_{0.5}TiO_3$**"

Acknowledgments

We sincerely appreciated the financial support by the Talent Fund Project of Southwest University of Science and Technology (21zx7104).

References

[1] C.F. Tseng, Microwave dielectric properties of a new $Cu_{0.5}Ti_{0.5}NbO_4$ ceramics, J. Eur. Ceram. Soc. 35 (1) (2015) 383–387.

[2] L.Z. Ni, L.X. Li, M.K. Du, et al., Wide temperature stable $Ba(Mg_xTa_{2/3})O_3$ microwave dielectric ceramics with ultra-high-Q applied for 5G dielectric filter, Ceram. Int. 47 (1) (2021) 1034–1039.

[3] L.Z. Ni, L.X. Li, M.K. Du, et al., Ultra-high-Q and wide temperature stable $Ba(Mg_{1/3}Ta_x)O_3$ microwave dielectric ceramic for 5G-oriented dielectric duplexer adhibition, J. Alloys Compd. 844 (2020) 156106.

[4] T. Yue, L.X. Li, M.K. Du, et al., Multilayer co-fired microwave dielectric ceramics in $MgTiO_3$-Li_2TiO_3 system with linear temperature coefficient of resonant frequency, Scripta Mater. 205 (2021) 114185.

[5] J. Zhang, Z.X. Yue, Y. Luo, et al., $MgTiO_3/TiO_2/MgTiO_3$: an ultrahigh-Q and temperature-stable microwave dielectric ceramic through cofired trilayer architecture, Ceram. Int. 44 (17) (2018) 21000–21003.

[6] M. Xin, L.M. Zhang, Y. Chang, et al., Influence of Sb_2O_3-ZnO additives on sintering characteristics and dielectric properties of $(Mg_{0.95}Ca_{0.05})TiO_3$ microwave ceramics, Ceram. Int. 44 (14) (2018) 17107–17112.

[7] A.G. Belous, O. Ovchar, D.A. Durilin, et al., High-Q microwave dielectric materials based on the spinel Mg_2TiO_4, J. Am. Ceram. Soc. 89 (11) (2006) 3441–3445.

[8] K.G. Wang, H.F. Zhou, X.W. Luan, et al., $NaTaO_3$ microwave dielectric ceramic a with high relative permittivity and as an excellent compensator for the temperature coefficient of resonant frequency, Ceram. Int. 47 (1) (2021) 121–129.

[9] S. Rabha, P. Dobbidi, Structural, electrical properties and stability in microwave dielectric properties of (1-*x*)$MgTiO_3$-*x*$SrTiO_3$ composite ceramics, J. Alloys Compd. 872 (2021) 159726.

[10] J.Y. Chen, C.L. Huang, A new low-loss microwave dielectric using $(Ca_{0.8}Sr_{0.2})TiO_3$-doped $MgTiO_3$ ceramics, Mater. Lett. 64 (23) (2010) 2585–2588.

[11] C.L. Huang, S.S. Liu, High-Q microwave dielectric in the (1-*x*)$MgTiO_3$–*x*$Ca_{0.6}La_{0.8/3}TiO_3$ ceramic system with a near-zero temperature coefficient of the resonant frequency, Mater. Lett. 62 (17) (2008) 3205–3208.

[12] C.L. Huang, K.H. Chiang, Structures and dielectric properties of a new dielectric material system *x*$MgTiO_3$-(1-*x*)$MgTa_2O_6$ at microwave frequency, J. Alloys Compd. 431 (1) (2006) 326–330.

[13] L.X. Li, S. Li, T. Tian, et al., Microwave dielectric properties of (1-*x*)$MgTiO_3$-*x*$(Ca_{0.6}Na_{0.2}Sm_{0.2})TiO_3$ ceramic system, J. Mater. Sci. Mater. Electron. 27 (2) (2016) 1286–1292.

[14] H. Jantunen, R. Rautioaho, A. usimäki, et al., Compositions of MgTiO3-CaTiO3 ceramic with two borosilicate glasses for LTCC technology, J. Eur. Ceram. Soc. 20 (14–15) (2000) 2331–2336.

[15] A. Belous, O. Ovchar, D. Durilin, et al., High-Q microwave dielectric materials based on the spinel Mg_2TiO_4, J. Am. Ceram. Soc. 89 (11) (2006) 3441–3445.

[16] H. Hu, W.Z. Lu, W. Lei, Microwave dielectric properties of the (1-*x*)Mg_2TiO_4-*x*$CaTiO_3$-ywt.% $ZnNb_2O_6$ ceramics system, Ceram. Int. 37 (5) (2011) 1515–1519.

[17] T. Yu, T. Luo, Q.H. Yang, et al., Ultra-high-quality factor of $Mg_6Ti_5O_{16}$-based microwave dielectric ceramics with temperature stability, J. Mater. Sci. Mater. Electron. 32 (2021) 2547–2556.

[18] J. Zhang, Y. Luo, Z.X. Yue, et al., Temperature stability, low loss and defect relaxation of MgO-TiO_2 microwave dielectric ceramics modified by $Ca_{0.8}Sr_{0.2}TiO_3$, Ceram. Int. 44 (1) (2018) 141–145.

[19] H.T. Yu, T. Luo, L. He, et al., Effect of ZnO on Mg_2TiO_4-$MgTiO_3$-$CaTiO_3$ microwave dielectric ceramics prepared by reaction sintering route, Adv. Appl. Ceram. 118 (2019) 98–105.

[20] Q. Hu, Y.C. Teng, X.F. Zhao, et al., Temperature stable dielectric properties of Mg_2TiO_4-$MgTiO_3$-$CaTiO_3$ ceramics over a wide temperature range, Ceram. Int. 49 (2) (2023) 1997–2006.

[21] N. Ichinose, K. Mutoh, Microwave dielectric properties in the (1-*x*)$(Na_{1/2}La_{1/2})TiO_3$-*x*$(Li_{1/2}Sm_{1/2})TiO_3$ ceramic system, J. Eur. Ceram. Soc. 23 (14) (2003) 2455–2459.

[22] C.L. Huang, G.J. Li, J.J. Wang, Microwave dielectric properties of (1-*x*)$(Mg_{0.95}Zn_{0.05})TiO_3$-*x*$(Na_{0.5}La_{0.5})TiO_3$ ceramic system, J. Alloys Compd. 472 (1–2) (2009) 497–501.

[23] B. Tang, L. Hao, F. Peng, et al., The effect of Mg: Ti ratio on the phase composition and microwave dielectric properties of $MgTiO_3$ ceramics prepared by one synthetic process, J. Mater. Sci. Mater. Electron. 25 (6) (2014) 2482–2486.

[24] S. Yuan, L. Gan, F. Ning, et al., High-Q×*f* 0.95$MgTiO_3$-0.05$CaTiO_3$ microwave dielectric ceramics with the addition of LiF sintered at medium temperatures, Ceram. Int. 44 (16) (2018) 20566–20569.

[25] Q. Hu, Y.C. Teng, X.F. Zhao, et al., Effect of Ni substituted $ZnZrTa_2O_8$ ceramics on crystal structure and microwave dielectric properties, J. Mater. Sci. Mater. Electron. 34 (2023) 676.

[26] I. Noboru, S. Takeshi, Effect of grain size and secondary phase on microwave dielectric properties of $Ba(Mg_{1/3}Ta_{2/3})O_3$ and $Ba([Mg,Zn]_{1/3}Ta_{2/3})O_3$ systems, J. Eur. Ceram. Soc. 26 (10–11) (2006) 1755–1759.

[27] K. Wang, H. Zhou, X. Liu, et al., A lithium aluminium borate composite microwave dielectric ceramic with low permittivity, near-zero shrinkage, and low sintering temperature, J. Eur. Ceram. Soc. 39 (4) (2019) 1122–1126.

[28] L. Hao, B. Tang, Y.X. Li, et al., Relationships between Sn substitution for Ti and microwave dielectric properties of $Mg_2(Ti_{1-x}Sn_x)O_4$ ceramics system, J. Mater. Sci. Mater. Electron. 26 (1) (2015) 571–577.

[29] X.B. Jia, Y. Xu, P. Zhao, et al., Structural dependence of microwave dielectric properties in ilmenite-type $Mg(Ti_{1-x}Nb_x)O_3$ solid solutions by Rietveld refinement and Raman spectra, Ceram. Int. 47 (5) (2021) 4820–4830.

[30] D. Zemlyanov, B. Aszalos-Kiss, E. Kleimenov, et al., In situ XPS study of Pd (111) oxidation. Part 1: 2D oxide formation in 10^3 mbar O_2, Surf. Sci. 600 (5) (2006) 983–994.

[31] A. Ghobadi, T.G. Ulusoy, R. Garifullin, et al., A heterojunction design of single layer hole tunneling ZnO passivation wrapping around TiO_2 nanowires for superior photocatalytic performance, Sci. Rep. 6 (1) (2016) 1–15.

[32] D. Pukazhselvan, N. Nasani, T. Yang, et al., Chemically transformed additive phases in Mg_2TiO_4 and $MgTiO_3$ loaded hydrogen storage system MgH_2, Appl. Surf. Sci. 472 (APR.1) (2018) 99–104.

[33] E.S. Kim, S.N. Seo, Dependence of dielectric properties on structural characteristics of $(Zn_{1/3}A_{2/3})_{0.5}(Ti_{1-x}B_x)_{0.5}O_2$ (A=Nb^{5+}, Ta^{5+}, B=Ge^{4+}, Sn^{4+}) ceramics at microwave frequencies, J. Eur. Ceram. Soc. 30 (2) (2010) 319–323.

[34] H. Zhu, W.Z. Lu, W. Lei, Microwave dielectric properties of the (1-*x*)Mg_2TiO_4-*x*$CaTiO_3$-ywt.%$ZnNb_2O_6$ ceramics system, Ceram. Int. 37 (5) (2011) 1515–1519.

[35] P. Gogoi, R.L. Singh, D. Pamu, Characterization of Zn doped $MgTiO_3$ ceramics: an approach for RF capacitor applications, J. Mater. Sci. Mater. Electron. 28 (16) (2017) 11712–11721.

[36] C. Wang, J. Hai, W. Feng, et al., Assignment of Raman-active vibrational modes of $MgTiO_3$, J. Appl. Phys. 104 (3) (2008), 034112-034112-6.

[37] H. Li, R. Xiang, X.Q. Chen, et al., Intrinsic dielectric behavior of Mg_2TiO_4 spinel ceramic, Ceram. Int. 46 (4) (2020) 4235–4239.

[38] E.S. Kim, C.J. Jeon, Microwave dielectric properties of $ATiO_3$ (A = Ni, Mg, Co, Mn) ceramics, J. Eur. Ceram. Soc. 30 (2) (2010) 341–346.

[39] X. Zhang, C. Liu, L. Shi, et al., Ti^{4+} modified $MgZrNb_2O_8$ microwave dielectric ceramics with an ultra-high-quality factor, J. Am. Ceram. Soc. 104 (11) (2021) 6054–6063.

[40] L. Shi, D.N. Zhang, R. Peng, et al., Investigation of crystal characteristics, Raman spectra, and microwave dielectric properties of $Mg_{1-x}Zn_xTa_2O_6$ ceramics, J. Eur. Ceram. Soc. 41 (11) (2021) 5526–5530.

[41] Y.J. Qian, H. Su, X.L. Tang, et al., Temperature stability of low-temperature fired (1-*x*)$ZnTiNb_2O_8$-*x*$CuTiNb_2O_8$ microwave dielectric ceramics, Ceram. Int. 47 (17) (2021) 24823–24830.

[42] A. Belous, O. Ovchar, D. Durilin, et al., High-Q microwave dielectric materials based on the spinel Mg_2TiO_4, J. Am. Ceram. Soc. 89 (11) (2006) 3441–3445.

[43] L. Hao, B. Tang, Y. Li, et al., Effects of $Mg_{2.05}SiO_{4.05}$ addition on phase structure and microwave properties of $MgTiO_3$-$CaTiO_3$ ceramic system, Mater. Lett. 145 (15) (2015) 30–33.

[44] G.G. Yao, C.D. Hou, C.J. Pei, et al., Effects of $Mg(OH)_2$ on phase formation and microwave dielectric properties of $Mg_6Ti_5O_{16}$ ceramics, Ferroelectrics 536 (2019) 156–161.